

PAPER

Electrical measurement of red blood cell deformability on a microfluidic device†

Cite this: *Lab Chip*, 2013, 13, 3275

Yi Zheng,^{ab} John Nguyen,^a Chen Wang^{*de} and Yu Sun^{*abc}

This paper describes a microfluidic system and a technique for electrically measuring the deformability of red blood cells (RBCs). RBCs are deformed when they flow through a small capillary (microfluidic channel). The microfluidic device consists of two stages of microchannels as two measurement units for measuring cell size/volume and cell deformability. A low frequency voltage signal is established across the microfluidic channel, and electrical current signal is sampled continuously when RBCs pass through the measurement areas. *Mechanical opacity* is defined to mitigate the coupled effect of cell size/volume and deformability. The system performed tests on controlled, glutaraldehyde-treated, and heated RBCs using a number of driving pressures. The experimental results proved the capability of the system for distinguishing different RBC populations based on their deformability with a throughput of ~ 10 cells s^{-1} .

Received 5th April 2013,
Accepted 23rd May 2013

DOI: 10.1039/c3lc50427a

www.rsc.org/loc

Introduction

Red blood cells (RBCs) are highly deformable, allowing them to be able to travel through *in vivo* capillaries with diameters smaller than RBCs' size, which facilitates gas transfer between blood and tissues.^{1–3} Decrease in RBC deformability can disturb blood flow and oxygen delivery. Essentially, the deformability of RBCs is determined by the integrity and organization of the membrane cytoskeletal protein network and density, and the viscosity of the cytoplasm. Pathological condition changes may lead to significant alteration and reorganization of the protein networks, and consequently compromise RBCs' deformability.^{2,4,5} For example, the polymerized and deoxygenated hemoglobin in sickled RBCs causes deformability to decrease.⁶ In the case of malaria, the impaired deformability of RBCs is in association with the interruption of the cytoskeleton network by parasite invasion.⁷ In addition to an indicator for pathological states, RBC deformability can also serve as a criterion for stored/banked blood quality assessment.^{8,9}

Several standard tools can be applied to measuring RBC deformability. Atomic force microscopy (AFM) assesses the deformability of a cell by indenting/deforming the cell through physical contact.^{10,11} Micropipette aspiration applies a negative pressure through a glass micropipette to aspirate a cell patch for characterizing the cell's mechanical parameters.^{10,12} Optical tweezers stretch a cell by optically manipulating high-refractive-index dielectric beads attached to the cell membrane.^{10,13} These standard tools involve high operation complexity and have a limited testing speed of minutes per cell.

Hence, other techniques were developed for testing RBC deformability with improved speed and/or reduced operation complexity.^{14–16} When RBCs flow through capillaries, they are deformed by shear stress into a parachute-like shape.^{1,17} Accordingly, microfluidic channels were used to mimic human capillaries and study RBC deformability. Shear stress-induced cell deformation was captured *via* a high speed camera.^{3,18,19} The use of high-speed cameras also necessitates a microscope and a high intensity lighting system, making the system inevitably bulky and costly. Furthermore, present high-speed cameras have limited on-board memory, permitting only a few seconds of recording and thus, limiting testing throughput (number of cells per test). Post-processing of tens of GB image data is also time-consuming.

A Cell Transit Analyzer (CTA) consists of micropores that are smaller than RBCs. It measures cell transit time (*i.e.*, the time required by an RBC to pass through) *via* electrical resistance changes or high-speed imaging. This approach is able to provide an increased throughput and is capable of performing multi-parameter measurements, particularly when electrical measurement is used ($100\text{--}150$ cells s^{-1}).²⁰ Recently, the CTA approach has been adapted for assessing the

^aDepartment of Mechanical and Industrial Engineering, University of Toronto, Toronto, ON, Canada. E-mail: sun@mie.utoronto.ca; Fax: +1 416-978-7753; Tel: +1 416-946-0549

^bInstitute of Biomaterials and Biomedical Engineering, University of Toronto, Toronto, ON, Canada

^cDepartment of Electrical and Computer Engineering, University of Toronto, Toronto, ON, Canada

^dDepartment of Pathology and Laboratory Medicine, Mount Sinai Hospital, Toronto, ON, Canada. E-mail: cwang@mtsinai.on.ca; Tel: +1 416-586-4469

^eDepartment of Laboratory Medicine and Pathobiology, University of Toronto, Toronto, ON, Canada

† Electronic supplementary information (ESI) available. See DOI: 10.1039/c3lc50427a

deformability of other cell types, including human cancer cells.^{21–23} An important advantage of CTA is its simplicity;²⁴ however, cell volume variations and adhesion between the cell surface and channel walls are coupled with cell deformability, which together determine cell transit time.²⁰ In other words, cell transit time is not only determined by cell deformability but also the volume/size and membrane properties.

In ektacytometry, RBCs are deformed by shear stress, and laser diffraction patterns of RBCs are analyzed.^{25,26} Diluted blood is loaded into a small gap between two rotating plates. RBCs are allowed to settle for a period of time to form weak adhesion with the bottom surface of the test chamber. Shear stress (*e.g.*, 0.5–50 Pa) is controlled by varying the rotation rate of the plates. Elongation index of the RBCs is measured using laser diffractometry. Ektacytometers are relatively easy-to-use; however, the measurement principle is difficult to implement on a miniaturized device design. Importantly, different from a CTA wherein RBCs flow continuously, in ektacytometry, the throughput is determined by the imaging field of the view. This limits testing throughput to approximately 50–60 RBCs per test (LoRRca MaxSis user manual, Mechatronics Manufacturing B. V., Netherlands).

Due to the simplicity of electrical measurement, measuring RBC deformability electrically was attempted.²⁷ In this reported system, medium viscosity was modified to achieve sufficient shear stress. It was incapable of decoupling RBC volume/size from deformability. Thus, RBCs with larger diameters can be mistakenly determined to be more deformable. This paper presents a microfluidic system for electrically measuring RBC deformability. The microfluidic device has two measurement stages, with cross-sectional areas of $8\ \mu\text{m} \times 8\ \mu\text{m}$ and $5\ \mu\text{m} \times 5\ \mu\text{m}$, respectively. RBCs are pressure driven to flow through the microfluidic channels while electrical

current changes are measured *via* two Ag/AgCl electrodes. To mitigate the coupled effect from cell volume, *mechanical opacity* is defined as an indicator of RBC deformability.

Measurement principle

In the microchannels, RBCs change into a parachute-like shape under shear stress. The cell is stretched along the flow direction, resulting in gaps between the RBC membrane and microchannel walls.^{1,19,28–30} As shown in Fig. 1, a voltage signal (10 kHz@0.5 V_{pp}) is applied across the microfluidic channel. RBCs have a specific membrane capacitance value of $9 \pm 0.8\ \text{mF m}^{-2}$, and hence act as an insulated layer at low frequencies (*e.g.*, 10 kHz).^{21,31,32} When an RBC is inside the channel, a portion of the conductive medium/liquid is replaced. Thus, only the conductive medium within the gaps between the cell membrane and channel walls conducts current, which causes the current passing through the channel to decrease. For two RBCs with the same volume/size but different deformability, the more deformable RBC [Fig. 1(a)] is stretched more along the flow direction leaving larger gaps between the cell membrane and channel walls (*vs.* the less deformable RBC). Therefore, electrical current within the channel is less blocked (*vs.* [Fig. 1(b)]), and in the measured current profile, current decrease is smaller. In other words, current decrease in this case is correlated to RBC deformation (see ESI,† Fig. S1). However, in addition to deformability, current decrease is also dependent on RBC size/volume, since a larger RBC replaces a larger volume of conductive medium, and thus causes stronger current blockage (ESI,† Fig. S1).

In order to take the cell volume effect into account, our device design has two measurement units [Fig. 2(a)]. Two Ag/AgCl electrodes are inserted into the inlet and outlet ports *via*

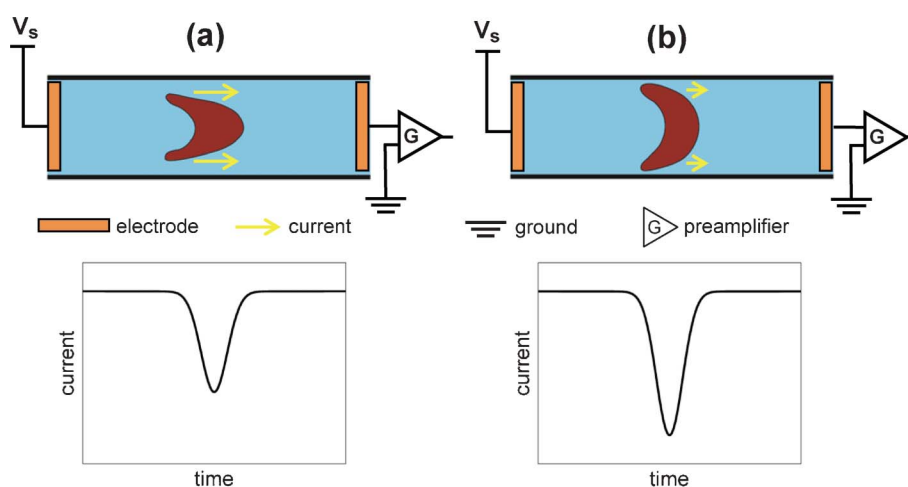


Fig. 1 Electrical measurement of RBC deformability. The schematics show two RBCs with identical size/volume but different deformability. A voltage signal is applied across the channel, and current (denoted as yellow arrows) is measured *via* a current preamplifier. Shear stress induces the RBCs into a parachute-like shape. The RBC with higher deformability is more stretched along the flow direction (a), resulting in larger gaps between the RBC membrane and channel walls than the less deformable RBC (b). Thus, the RBC with higher deformability blocks less current (*i.e.*, smaller current decrease in the current profile) than the RBC with lower deformability.

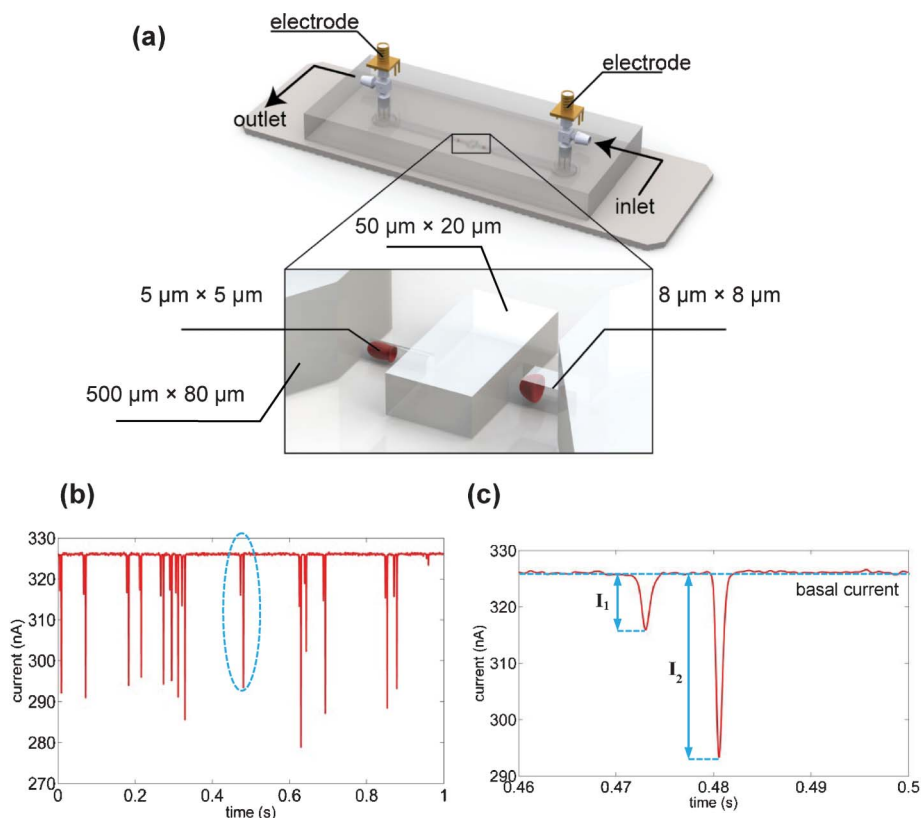


Fig. 2 (a) Microfluidic device for electrically measuring RBC size and deformability. Ag/AgCl electrodes are plugged into the inlet and outlet ports via T-junctions. The cross-sectional areas of the measurement units are $8\ \mu\text{m} \times 8\ \mu\text{m}$ and $5\ \mu\text{m} \times 5\ \mu\text{m}$, respectively. The transit region ($50\ \mu\text{m} \times 20\ \mu\text{m}$) is for separating the two current valleys of the two measurement units. RBCs are driven through the measurement areas continuously (see ESI Video 1†). (b) Experimental data: time series of the current profile measured within 1 s with 14 RBCs passing through. (c) The zoom-in view of the profile circled in (b).

T-junctions to apply a voltage signal and measure current changes. Custom-made water tanks were used to generate pressure for driving RBCs through the microchannels. The cross-sectional area of the first measurement unit is $8\ \mu\text{m} \times 8\ \mu\text{m}$, and the cross-sectional area of the second measurement unit is $5\ \mu\text{m} \times 5\ \mu\text{m}$. The transit region in between ($50\ \mu\text{m} \times 20\ \mu\text{m}$) is designed for separating the two current valleys [Fig. 2(b) and (c)] of the two measurement units for the convenience of signal processing. Fig. 2(b) shows experimental data that are time series of the current profile measured within 1 s with 14 RBCs passing through the measurement area under a pressure difference of 1600 Pa. The zoom-in view of the profile circled in Fig. 2(b) is presented in Fig. 2(c). The small valley (I_1) of the current profile corresponds to the current decrease when an RBC passed through the $8\ \mu\text{m} \times 8\ \mu\text{m}$ channel; and the large valley (I_2) was generated when the same RBC passed through the $5\ \mu\text{m} \times 5\ \mu\text{m}$ channel.

As discussed earlier in this section, the electrical current signals from both the $5\ \mu\text{m} \times 5\ \mu\text{m}$ channel and $8\ \mu\text{m} \times 8\ \mu\text{m}$ channel are dependent on cell volume and deformation. The shear stress within the $5\ \mu\text{m} \times 5\ \mu\text{m}$ channel is approximately four times as high as that in the $8\ \mu\text{m} \times 8\ \mu\text{m}$ channel. As a result, RBCs are much more deformed in the $5\ \mu\text{m} \times 5\ \mu\text{m}$ channel. Additionally, due to the smaller cross-sectional area,

current signal is more sensitive to changes of gaps between the cell membrane and channel walls in the $5\ \mu\text{m} \times 5\ \mu\text{m}$ channel. In the meanwhile, the current signal generated in the $8\ \mu\text{m} \times 8\ \mu\text{m}$ channel is more reflective of the RBCs volume information, as the Coulter counter principle.^{33,34} To mitigate the coupled effect from cell volume and cell deformability, the ratio of I_2/I_1 is defined in this study as *mechanical opacity*, and is used as a measure of RBC deformability. RBCs' 3D orientation is crucial for the measurement principle. In the $5\ \mu\text{m} \times 5\ \mu\text{m}$ microchannel, all the RBCs present a parachute-like shape (*i.e.*, same orientation) due to the confinement effect¹⁹ (see ESI Video 1†).

Materials and methods

Blood sample preparation

Whole blood samples were obtained from healthy donors (MCV: 85–95 fL; MCH: 27–31 pg; hematocrit: 40–50%) (Mount Sinai Hospital, Toronto, Canada). Blood samples were anticoagulated with EDTA anticoagulant (ethylenediaminetetraacetic acid $1.5\ \text{mg}\ \text{ml}^{-1}$) (Sigma-Aldrich, Oakville, ON, Canada) and washed twice with PBS (Sigma-Aldrich, Oakville, ON, Canada) before further treatment. Glutaraldehyde (GA)-treated

and heated RBCs have been commonly used in the literature for studying RBC deformability. GA is a nonspecific fixative that lowers RBC deformability by cross-linking the cytoskeletal proteins.¹⁸ Heating can significantly denature the RBC cytoskeletal network and make RBCs more deformable.³⁵ For glutaraldehyde (GA) treated samples, the washed RBCs were suspended into PBS added with 0.005% glutaraldehyde, and incubated at room temperature for 30 min. Following incubation with GA, the RBCs were washed three times with PBS. For heat treatment, the washed RBCs were re-suspended in a PBS solution and heated in a water bath maintained at 49 °C for 30 min. Thereafter, all RBCs samples were suspended in PBS with 1% w/v BSA with hematocrit of 0.45%, and incubated for 30 min at room temperature to prevent adhesion. No observable volume/size and morphology changes occurred after treatments.

Device fabrication and operation

The device was fabricated using standard multilayer soft lithography.^{22,36} The microfluidic channel consists of four different cross-section areas: two measurement units ($5\ \mu\text{m} \times 5\ \mu\text{m}$ and $8\ \mu\text{m} \times 8\ \mu\text{m}$); the transit unit ($50\ \mu\text{m} \times 20\ \mu\text{m}$) in between the two measurement units; and the loading channel ($500\ \mu\text{m} \times 80\ \mu\text{m}$) for loading RBCs to the measurement areas. Since the loading channel's cross-sectional area is much larger than the measurement units, electrical current is largely determined by the resistance of the measurement areas. Before experiments, the microchannel was incubated with PBS (Sigma-Aldrich, Oakville, ON, Canada) mixed with 0.2% w/v Pluronic (Sigma-Aldrich, Oakville, ON, Canada) and 1% w/v BSA (New England Biolabs Inc., Herts, UK) for 30 min. A droplet of RBC sample was pipetted into the inlet port of the device. The two T-junctions with Ag/AgCl non-polarizable electrodes were then inserted. The T-junctions were connected with custom-made water tanks for accurately generating pressure differences.

Signal processing

A sinusoidal voltage signal (10 kHz@0.5 V_{pp}) was applied through the Ag/AgCl electrodes. A current preamplifier connected in series into the current pathway, amplified and converted current into voltage signals, which are sampled by a computer. When RBCs flow through the measurement units, current (RMS) is measured continuously, as shown in Fig. 2(b) and (c). At low frequencies, the electrical current signal can better reflect RBCs deformation since current cannot penetrate the RBC membrane. The frequency of 10 kHz was chosen as a compromise of system time response and deformation measurement sensitivity. Experimental data was processed using a custom-built program. Briefly, basal current was extracted from the raw data using a histogram-based technique. Peak threshold values were calculated as 98% the basal current. Peak detection was conducted after noise filtering. The blood samples used in experiments were from whole blood and contained white blood cells (WBCs) and platelets. In the data processing, WBCs and platelets were excluded from the final results on the basis of distinct current signals (see ESI,† Fig. S2). Data processing also excluded the rare events with multiple cells within the measurement unit, where

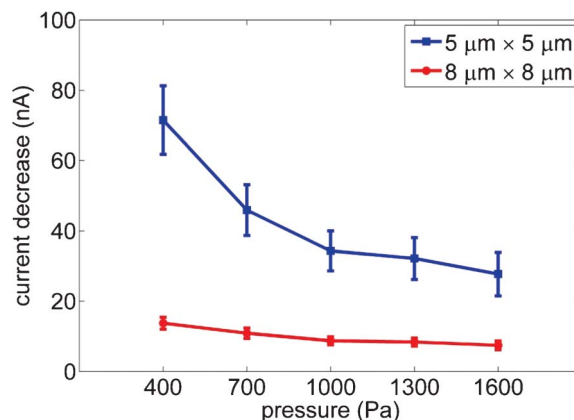


Fig. 3 Current decrease within $8\ \mu\text{m} \times 8\ \mu\text{m}$ measurement unit (I_1 , red) and $5\ \mu\text{m} \times 5\ \mu\text{m}$ measurement unit (I_2 , blue) of a controlled RBC sample under various driving pressures. The error bars represent standard deviation. More than 1000 RBCs were measured for each data point.

consecutive large valleys appear in the measured data (see ESI,† Fig. S2).

Results and discussion

Shear stress effect

The pressure difference generated with the water tanks ranged from 400 Pa to 1600 Pa. The corresponding average shear stress in the $5\ \mu\text{m} \times 5\ \mu\text{m}$ channel was approximately 8 Pa to 36 Pa (ESI,† Fig. S3). This pressure range was tested to make a comparison with the results from commercial ektacytometers (shear stress range 0.5–50 Pa). A controlled RBC sample was tested under several pressures (400 Pa, 700 Pa, 1000 Pa, 1300 Pa, 1600 Pa). The electrical current decrease of the $5\ \mu\text{m} \times 5\ \mu\text{m}$ channel (I_2 , blue) and $8\ \mu\text{m} \times 8\ \mu\text{m}$ channel (I_1 , red) under these pressures is summarized in Fig. 3. When an RBC is in the $5\ \mu\text{m} \times 5\ \mu\text{m}$ channel, current change is highly sensitive to pressure since under increasing pressures, the RBC is further stretched along the flow direction. While in the $8\ \mu\text{m} \times 8\ \mu\text{m}$ channel, shear stress is lower, and current change is far less sensitive to pressure variations.

Ideally, the first measurement unit should be much larger than the size of RBCs so that the low shear stress hardly deforms a cell, and the current signal is only determined by cell volume/size. However, too large a cross-sectional area in the Coulter counter measurement unit in experiments caused too small a current change when a cell passed through. Therefore, $8\ \mu\text{m} \times 8\ \mu\text{m}$ was chosen to achieve a reasonable signal-to-noise ratio and reduce the cell deformation effect on the measured signal. As shown in Fig. 3, although the measured signal shows slight changes as the applied pressure increases, the change is much less significant than the signal generated in the $5\ \mu\text{m} \times 5\ \mu\text{m}$ channel. Further size reduction of the $5\ \mu\text{m} \times 5\ \mu\text{m}$ channel would increase the system's basal resistance and cause difficulties to distinguish I_1 from noise. In the $5\ \mu\text{m} \times 5\ \mu\text{m}$ channel, current signal is determined by the gaps between RBC membrane and the channel walls.

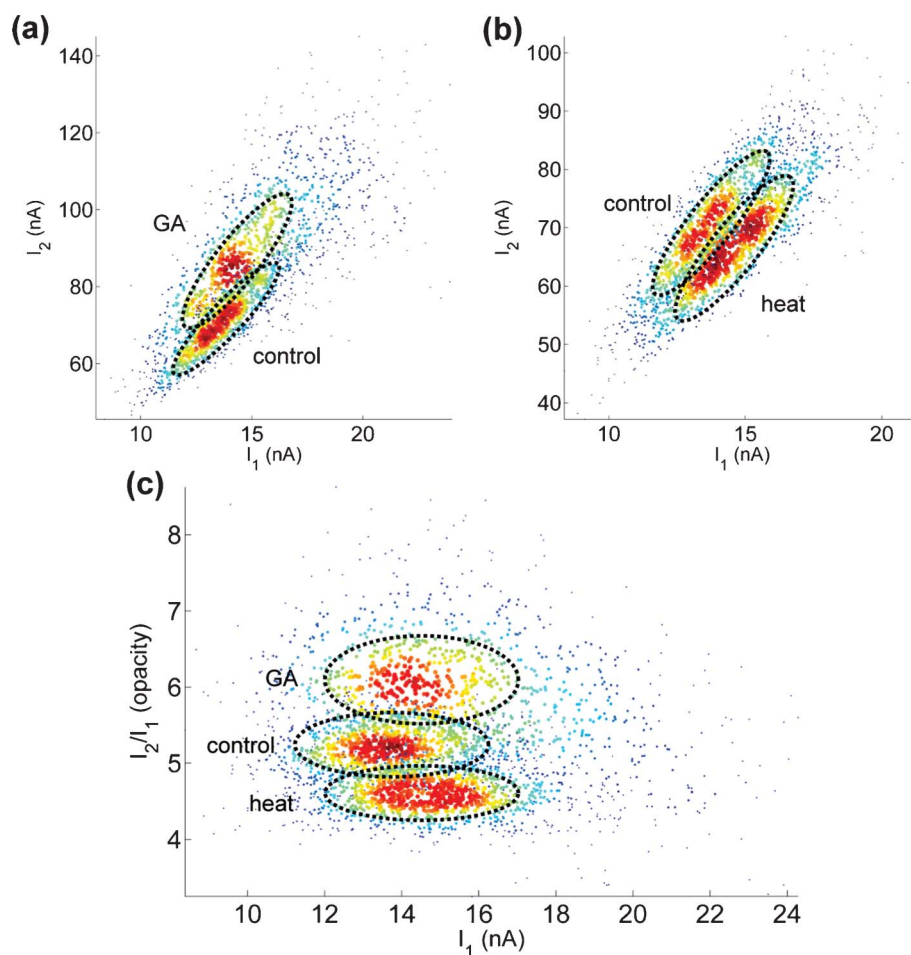


Fig. 4 (a) Scatter plot of I_2 vs. I_1 for controlled RBCs ($n = 996$) and GA-treated RBCs ($n = 1059$). (b) Scatter plot of I_2 vs. I_1 for controlled RBCs ($n = 996$) and heated RBCs ($n = 1179$). All RBCs were measured under a driving pressure of 400 Pa. I_2 depends linearly on I_1 . For RBCs with the same I_1 , GA-treated RBCs and heated RBCs show a higher and lower I_2 than controlled RBCs, respectively. (c) Scatter plot of I_2/I_1 (opacity) vs. I_1 for controlled, GA-treated and heated RBCs. RBCs deformability is reflected by the ratio of I_2/I_1 . The data show that GA treatment decreases RBC deformability and heat treatment increases RBC deformability.

However, it is challenging to experimentally measure the gaps using standard microscope imaging.

Mechanical opacity

Controlled, GA-treated, and heated RBCs were tested using this system. The scatter plots show I_2 versus I_1 for controlled RBCs and GA-treated RBCs [Fig. 4(a)], and controlled RBCs and heated RBCs [Fig. 4(b)]. The driving pressure was 400 Pa. In Fig. 4(a) and (b), I_2 shows a strong linear correlation with I_1 . Comparing the controlled RBCs and GA-treated RBCs with the same I_1 value (volume indicator), the GA-treated RBCs have clearly higher I_2 values, reflecting the fact that the controlled RBCs are more deformable than the GA-treated RBCs because they are stretched more along the flow direction (larger gaps). The heated RBCs reveal a lower I_2 , indicating heated RBCs are more deformable than controlled RBCs. Here, we borrow the concept of impedance opacity (*i.e.*, ratio of impedance at high frequency to low frequency) from impedance flow cytometry.^{37,38} Due to the strong linear dependence, the ratio of I_2/I_1 was thereby used to normalize RBC volume, which is defined as *mechanical opacity*. Based on the mechanical opacity that

reflects RBC deformability, GA-treated RBCs and heated RBCs can be effectively separated from controlled RBCs [Fig. 4(c)]. Mechanical opacity (I_2/I_1) and I_1 reflect the RBCs' deformability and volume/size, respectively.

System characterization

Fig. 5(a) and (b) shows the histograms of I_2/I_1 (opacity) of controlled, GA-treated, and heated RBCs measured under 400 Pa and 1600 Pa, fitted with normalized distribution. These two pressures were chosen as representatives of low and high pressure. As expected, the less deformable population (GA-treated) shows an opacity distribution shifted to the right, and the more deformable population (heated) shows a left shifted opacity distribution, compared to the controlled population. It was also found that the GA-treated RBCs have a wider distribution compared to controlled and heated RBCs. As driving pressure increases [Fig. 5(b)], the difference in the average opacity values among the populations becomes smaller, implying lower sensitivity for distinguishing the three populations. Fig. 5(c) summarizes the ratio of I_2/I_1 (opacity) of controlled RBCs (red), GA-treated RBCs (blue), and heated

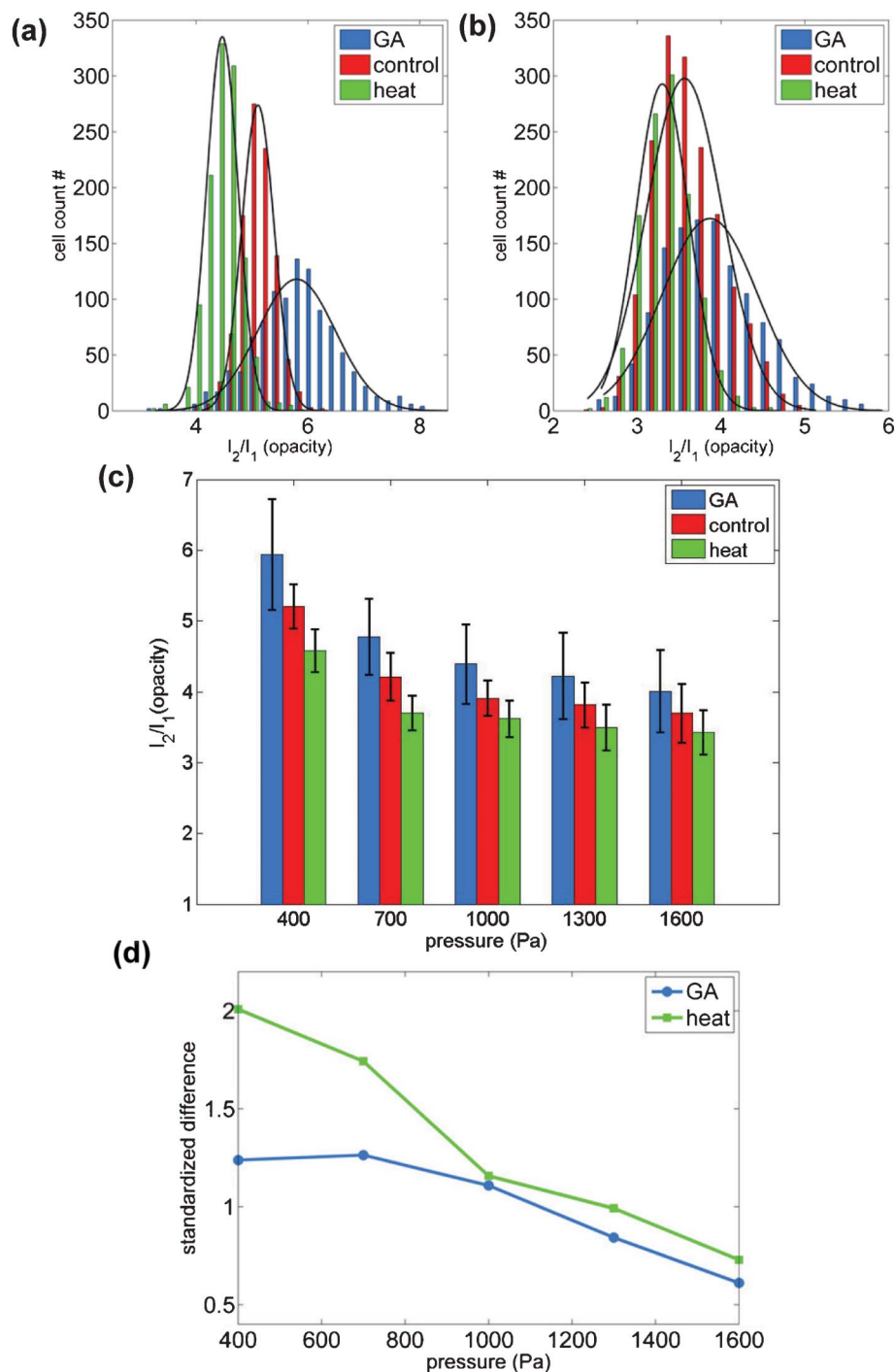


Fig. 5 Histograms of I_2/I_1 (opacity) of controlled, GA-treated and heated RBCs under (a) 400 Pa and (b) 1600 Pa driving pressures, fitted with normalized distribution. (c) Mechanical opacity of controlled RBCs (red), GA-treated RBCs (blue) and heated RBCs (green) measured under different driving pressures. Results are mean \pm standard deviation. More than 1000 RBCs were tested for each of the data points. (d) Standardized difference values calculated using the data present in (c). Blue: standardized difference between GA-treated and controlled RBCs. Green: standardized difference between heated and controlled RBCs.

RBCs (green) measured under different driving pressures. The GA-treated RBCs (less deformable) shows consistently higher mechanical opacity than controlled RBCs while heated RBCs consistently have lower mechanical opacity values (more deformable). As driving pressure increased, the difference between different populations became smaller. *P*-values of the

two-group *T*-test show statistically significant difference between the controlled and treated RBCs at all applied pressure ($p < 0.05$).

To evaluate the power to detect differences between controlled and treated RBCs, standardized difference values

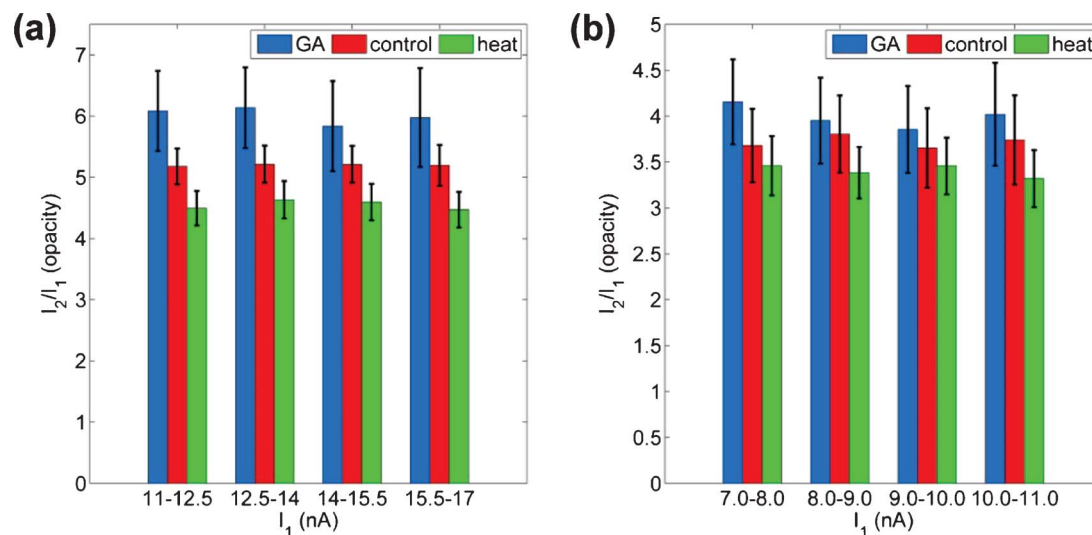


Fig. 6 Comparison of I_2/I_1 (opacity) of controlled, GA-treated, and heated RBCs within sub-ranges of I_1 . (a) 400 Pa driving pressure, (b) 1600 Pa driving pressure. Error bars represent standard deviation.

in comparison with controlled RBCs were calculated according to

$$SD = \frac{(X_1 - X_2)}{\sqrt{\frac{(S_1^2 + S_2^2)}{2}}}$$

where X_1 , X_2 and S_1 , S_2 denote the sample mean, standard deviation of each group, respectively.

As shown in Fig. 5(d), standardized difference values of both GA-treated and heated RBCs decrease as the driving pressure increases. This finding is in agreement with the results generated using ektacytometry.^{39,40} Ektacytometry results showed that RBC deformation became less sensitive as shear stress increased from several Pa to 30 Pa, which caused lower standardized difference values.

We further investigated the effect of RBC volume on the measured mechanical opacity. Fig. 6(a) and (b) shows the average and standard deviation of measured mechanical opacity for different ranges of I_1 , under 400 Pa and 1600 Pa, respectively. Since I_1 is an indicator of RBC volume, comparing *mechanical opacity* values within each I_1 sub-range could reveal the deformability of RBCs within the same size group. For each RBC population (controlled, GA-treated, and heated), the *mechanical opacity* values across the four size (I_1) sub-ranges are all close to the population's overall average value; the standard deviation of all controlled, GA-treated and heated RBCs show very little variation across the four sub-ranges. These results indicate that the *mechanical opacity* quantity mitigates the coupled effect from RBC volume and reflects RBC deformability.

Conclusion

This paper presented a microfluidic system for electrically measuring RBC deformability. The two-stage device design

and measurement technique together mitigate the cell volume effect on RBC deformability. By measuring controlled, GA-treated and heated RBCs, the system demonstrated the capability of distinguishing RBC populations having known deformability differences. The electrical measurement system has a speed of 10–20 cells per second. The speed can be further improved by increasing cell density and driving pressure. However, as shown in Fig. 5, the ability to distinguish different populations would decrease at higher driving pressures.

Acknowledgements

Financial support from the Natural Sciences and Engineering Research Council of Canada (NSERC) through an E. W. R. Steacie Fellowship, from the University of Toronto through a Connaught Innovation Award, and from the Canada Research Chairs Program is acknowledged.

References

- 1 M. Abkarian, M. Faivre, R. Horton, K. Smistrup, C. A. Best-Popescu and H. A. Stone, Cellular-scale hydrodynamics, *Biomed. Mater.*, 2008, **3**, 034011.
- 2 M. Diez-Silva, M. Dao, J. Y. Han, C. T. Lim and S. Suresh, Shape and biomechanical characteristics of human red blood cells in health and disease, *MRS Bull.*, 2010, **35**, 382–388.
- 3 G. Tomaiuolo, M. Barra, V. Preziosi, A. Cassinese, B. Rotoli and S. Guido, Microfluidics analysis of red blood cell membrane viscoelasticity, *Lab Chip*, 2011, **11**, 449–454.
- 4 D. E. Discher, New insights into erythrocyte membrane organization and microelasticity, *Curr. Opin. Hematol.*, 2000, **7**, 117–122.

- 5 G. Y. H. Lee and C. T. Lim, Biomechanics approaches to studying human diseases, *Trends Biotechnol.*, 2007, **25**, 111–118.
- 6 S. H. Embury, R. P. Hebbel, M. H. Steinberg and N. Mohandas, *Pathogenesis of vasoocclusion*, Raven Press {a}, New York, USA, 1994.
- 7 J. P. Mills, M. Diez-Silva, D. J. Quinn, M. Dao, M. J. Lang, K. S. W. Tan, C. T. Lim, G. Milon, P. H. David, O. Mercereau-Puijalon, S. Bonnefoy and S. Suresh, Effect of plasmodial RESA protein on deformability of human red blood cells harboring *Plasmodium falciparum*, *Proc. Natl. Acad. Sci. U. S. A.*, 2007, **104**, 9213–9217.
- 8 J. Bonaventura, Clinical implications of the loss of vasoactive nitric oxide during red blood cell storage, *Proc. Natl. Acad. Sci. U. S. A.*, 2007, **104**, 19165–19166.
- 9 E. Bennett-Guerrero, T. H. Veldman, A. Doctor, M. J. Telen, T. L. Ortel, T. S. Reid, M. A. Mulherin, H. Zhu, R. D. Buck, R. M. Califf and T. J. McMahon, Evolution of adverse changes in stored RBCs, *Proc. Natl. Acad. Sci. U. S. A.*, 2007, **104**, 17063–17068.
- 10 D. H. Kim, P. K. Wong, J. Park, A. Levchenko and Y. Sun, Microengineered platforms for cell mechanobiology, *Annu. Rev. Biomed. Eng.*, 2009, **11**, 203–233.
- 11 O. Loh, A. Vaziri and H. Espinosa, The potential of MEMS for advancing experiments and modeling in cell mechanics, *Exp. Mech.*, 2009, **49**, 105–124.
- 12 R. M. Hochmuth, Micropipette aspiration of living cells, *J. Biomech.*, 2000, **33**, 15–22.
- 13 S. Suresh, Biomechanics and biophysics of cancer cells, *Acta Biomater.*, 2007, **3**, 413–438.
- 14 X. L. Mao and T. J. Huang, Exploiting mechanical biomarkers in microfluidics, *Lab Chip*, 2012, **12**, 4006–4009.
- 15 S. A. Vanapalli, M. H. G. Duits and F. Mugele, Microfluidics as a functional tool for cell mechanics, *Biomicrofluidics*, 2009, **3**, 012006.
- 16 Y. Zheng and Y. Sun, Microfluidic devices for mechanical characterisation of single cells in suspension, *Micro Nano Lett.*, 2011, **6**, 327–331.
- 17 K. Tsukada, E. Sekizuka, C. Oshio and H. Minamitani, Direct measurement of erythrocyte deformability in diabetes mellitus with a transparent microchannel capillary model and high-speed video camera system, *Microvasc. Res.*, 2001, **61**, 231–239.
- 18 A. M. Forsyth, J. D. Wan, W. D. Ristenpart and H. A. Stone, The dynamic behavior of chemically stiffened red blood cells in microchannel flows, *Microvasc. Res.*, 2010, **80**, 37–43.
- 19 G. Tomaiuolo, M. Simeone, V. Martinelli, B. Rotoli and S. Guido, Red blood cell deformation in microconfined flow, *Soft Matter*, 2009, **5**, 3736–3740.
- 20 Y. Zheng, E. Shojaei-Baghini, A. Azad, C. Wang and Y. Sun, High-throughput biophysical measurement of human red blood cells, *Lab Chip*, 2012, **12**, 2560–7.
- 21 A. Adamo, A. Sharei, L. Adamo, B. Lee, S. Mao and K. F. Jensen, Microfluidics-based assessment of cell deformability, *Anal. Chem.*, 2012, **84**, 6438–6443.
- 22 J. Chen, Y. Zheng, Q. Y. Tan, E. Shojaei-Baghini, Y. L. Zhang, J. Li, P. Prasad, L. D. You, X. Y. Wu and Y. Sun, Classification of cell types using a microfluidic device for mechanical and electrical measurement on single cells, *Lab Chip*, 2011, **11**, 3174–3181.
- 23 H. W. Hou, Q. S. Li, G. Y. H. Lee, A. P. Kumar, C. N. Ong and C. T. Lim, Deformability study of breast cancer cells using microfluidics, *Biomed. Microdevices*, 2009, **11**, 557–564.
- 24 D. Di Carlo, A mechanical biomarker of cell state in medicine, *Jala*, 2012, **17**, 32–42.
- 25 M. R. Hardeman, G. A. J. Besselink, I. Ebbing, D. de Korte, C. Ince and A. J. Verhoeven, Laser-assisted optical rotational cell analyzer measurements reveal early changes in human RBC deformability induced by photodynamic treatment, *Transfusion*, 2003, **43**, 1533–1537.
- 26 S. Shin, J. X. Hou, J. S. Suh and M. Singh, Validation and application of a microfluidic ektacytometer (RheoScan-D) in measuring erythrocyte deformability, *Clinical Hemorheology and Microcirculation*, 2007, **37**, 319–328.
- 27 Y. Katsumoto, K. Tatsumi, T. Doi and K. Nakabe, Electrical classification of single red blood cell deformability in high-shear microchannel flows, *Int. J. Heat Fluid Flow*, 2010, **31**, 985–995.
- 28 J. H. Jeong, Y. Sugii, M. Minamiyama and K. Okamoto, Measurement of RBC deformation and velocity in capillaries in vivo, *Microvasc. Res.*, 2006, **71**, 212–217.
- 29 G. Tomaiuolo and S. Guido, Start-up shape dynamics of red blood cells in microcapillary flow, *Microvasc. Res.*, 2011, **82**, 35–41.
- 30 T. Ye, H. Li and K. Y. Lam, Modeling and simulation of microfluid effects on deformation behavior of a red blood cell in a capillary, *Microvasc. Res.*, 2010, **80**, 453–463.
- 31 D. Holmes and H. Morgan, Single cell impedance cytometry for identification and counting of CD4 T-cells in human blood using impedance labels, *Anal. Chem.*, 2010, **82**, 1455–1461.
- 32 Y. Zheng, E. Shojaei-Baghini, C. Wang and Y. Sun, Microfluidic characterization of specific membrane capacitance and cytoplasm conductivity of single cells, *Biosens. Bioelectron.*, 2012, **42**, 496–502.
- 33 H. Choi, K. B. Kim, C. S. Jeon, I. Hwang, S. A. Lee, H. K. Kim, H. C. Kim and T. D. Chung, A label-free DC impedance-based microcytometer for circulating rare cancer cell counting, *Lab Chip*, 2013, **13**, 970–977.
- 34 J. Riordon, M. Mirzaei and M. Godin, Microfluidic cell volume sensor with tunable sensitivity, *Lab Chip*, 2012, **12**, 3016–3019.
- 35 Y. H. Zhan, D. N. Loufakis, N. Bao and C. Lu, Characterizing osmotic lysis kinetics under microfluidic hydrodynamic focusing for erythrocyte fragility studies, *Lab Chip*, 2012, **12**, 5063–5068.
- 36 Y. Zheng, E. Shojaei-Baghini, C. Wang and Y. Sun, Microfluidic characterization of specific membrane capacitance and cytoplasm conductivity of single cells, *Biosens. Bioelectron.*, 2013, **42**, 496–502.
- 37 K. C. Cheung, M. Di Berardino, G. Schade-Kampmann, M. Hebeisen, A. Pierzchalski, J. Bocsi, A. Mittag and A. Tarnok, Microfluidic impedance-based flow cytometry, *Cytometry, Part A*, 2010, **77A**, 648–666.
- 38 D. Holmes, D. Pettigrew, C. H. Reccius, J. D. Gwyer, C. van Berkel, J. Holloway, D. E. Davies and H. Morgan, Leukocyte analysis and differentiation using high speed microfluidic single cell impedance cytometry, *Lab Chip*, 2009, **9**, 2881–2889.

- 39 O. K. Baskurt, T. C. Fisher and H. J. Meiselman, Sensitivity of the cell transit analyzer (CTA) to alterations of red blood cell deformability: Role of cell size pore size ratio and sample preparation, *Clinical Hemorheology*, 1996, **16**, 753–765.
- 40 O. K. Baskurt, M. R. Hardeman, M. Uyklu, P. Ulker, M. Cengiz, N. Nemeth, S. Shin, T. Alexy and H. J. Meiselman, Comparison of three commercially available ektacytometers with different shearing geometries, *Biorheology*, 2009, **46**, 251–264.